MOLECULAR AND CELLULAR BIOLOGY, Dec. 2004, p. 10703–10717 Vol. 24, No. 24
0270-7306/04/$08.00+0 DOI: 10.1128/MCB.24.24.10703–10717.2004

NAD(P)H Oxidase Nox-4 Mediates 7-Ketocholesterol-Induced Endoplasmic Reticulum Stress and Apoptosis in Human Aortic Smooth Muscle Cells

Eric Pedruzzi,[1] Cécile Guichard,[1] Véronique Ollivier,[1] Fathi Driss,[2] Michèle Fay,[1] Céline Prunet,[3] Jean-Claude Marie,[4] Cécile Pouzet,[5] Mohammad Samadi,[6] Carole Elbim,[1] Yvonne O'Dowd,[1] Marcelle Bens,[7] Alain Vandewalle,[7] Marie-Anne Gougerot-Pocidalo,[1] Gérard Lizard,[3]† and Eric Ogier-Denis[1]†*

INSERM U479,[1] INSERM U410,[4] and INSERM U478,[7] Faculté de Médecine Xavier Bichat, Hôpital X. Bichat, Service de Biochimie Hormonale et Génétique,[2] and IFR02, Paris,[5] LIMBP Faculté des Sciences, Université de Metz, Ile de Saulcy, Metz,[6] and INSERM U498 CHU du Bocage, Laboratoire de Biochimie Médicale, Dijon,[3] France

Received 5 August 2004/Accepted 9 September 2004

The mechanisms involved in the cytotoxic action of oxysterols in the pathogenesis of atherosclerosis still remain poorly understood. Among the major oxysterols present in oxidized low-density lipoprotein, we show here that 7-ketocholesterol (7-Kchol) induces oxidative stress and/or apoptotic events in human aortic smooth muscle cells (SMCs). This specific effect of 7-Kchol is mediated by a robust upregulation (threefold from the basal level) of Nox-4, a reactive oxygen species (ROS)-generating NAD(P)H oxidase homologue. This effect was highlighted by silencing Nox-4 expression with a specific small interfering RNA, which significantly reduced the 7-Kchol-induced production of ROS and abolished apoptotic events. Furthermore, the 7-Kchol activating pathway included an early triggering of endoplasmic reticulum stress, as assessed by transient intracellular Ca^{2+} oscillations, and the induction of the expression of the cell death effector CHOP and of GRP78/Bip chaperone via the activation of IRE-1, all hallmarks of the unfolded protein response (UPR). We also showed that 7-Kchol activated the IRE-1/Jun-NH_2-terminal kinase (JNK)/AP-1 signaling pathway to promote Nox-4 expression. Silencing of IRE-1 and JNK inhibition downregulated Nox-4 expression and subsequently prevented the UPR-dependent cell death induced by 7-Kchol. These findings demonstrate that Nox-4 plays a key role in 7-Kchol-induced SMC death, which is consistent with the hypothesis that Nox-4/oxysterols are involved in the pathogenesis of atherosclerosis.

Atherosclerosis is a slow degenerative process and is the underlying cause of heart attacks, strokes, and peripheral artery diseases in humans. This complex disorder is characterized by a remodeling of the arterial wall, leading to the formation of an atherosclerotic plaque. Plaque formation is induced by the accumulation, at the subendothelial level, of oxidized low-density lipoproteins (LDLs) and subsequently of some of their lipid constituents (oxysterols, oxidized fatty acids, aldehydes, and lysophospholipids) and fibrous elements.

To date, a number of studies have shown that oxysterols constitute an important family of oxygenated derivatives of cholesterol that exert potent biological effects in the pathogenesis of atherosclerosis (for a review, see references 6 and 9). Among the oxysterols that have been identified, those oxidized at the C7 position, such as 7-ketocholesterol (7-Kchol), are the ones most frequently detected at high levels in atherosclerotic plaques (9) and in the plasma of patients with high cardiovascular risk factors (55). 7-Kchol exerts deleterious effects on vascular smooth muscle cells (SMCs), including the stimulation of reactive oxygen species (ROS) production (28) and the induction of apoptosis (30, 34, 42), two major events involved in atherogenesis. The oxidation of macromolecules (proteins, lipids, and DNA) and apoptosis induce the progression of atherosclerosis. Thus, the death of vascular SMCs and monocyte-derived foam cells has been shown to modulate the cellularity of the plaque (22, 31, 32) and is believed to play important roles in plaque growth, as well as in promoting procoagulation and plaque rupture (27).

Nonphagocytic NAD(P)H oxidase-dependent production of ROS is thought to be an important regulator of SMC viability and is believed to be linked to the development and severity of human atherosclerotic lesions (16). Recently, a new family of oxidases, known as the Nox family (named for NADPH oxidase) has been defined on the basis of their homology with the $gp91^{phox}$ catalytic subunit of phagocyte NAD(P)H oxidase. To date, four homologues (Nox-1, Nox-3, Nox-4, and Nox-5 with levels of identity with $gp91^{phox}$ [also known as Nox-2] of 58, 56, 37, and 27%, respectively) have been identified in human nonphagocytic cells (5, 11, 14, 23, 46). These homologues share with Nox-2 putative NAD(P)H and flavin-binding sites, as well as functional oxidase activity that produces the superoxide anion (14, 46). A large variety of cell types express multiple Nox proteins. Recent studies have demonstrated that the Nox-1, Nox-4, and Nox-5 homologues are mainly expressed in cultured vascular SMCs (25, 26). Within these cells, Nox activity is modulated by a variety of mediators detected in vascular diseases such as angiotensin II, thrombin, platelet-derived growth factor (PDGF), and tumor necrosis factor alpha

* Corresponding author. Mailing address: INSERM U479, Faculté de Médecine Xavier Bichat, BP416, 75870 Paris Cedex 18, France. Phone: 33-1-44-85-62-12. Fax: 33-1-44-85-62-07. E-mail: ogier@bichat.inserm.fr.

† G.L. and E.O.-D. contributed equally to this study.

(TNF-α). Coronary artery restenosis, a frequent complication of angioplasty, is accompanied by an increase in Nox-generated ROS production (44). Likewise, balloon injury of the carotid artery is known to result in an increase in ROS production throughout the vessel wall, and this is associated with an upregulation of Nox proteins. This increase in ROS appears to be derived from SMCs in the media and neointima of the arterial wall (47). However, the implication of oxysterols in the regulation of Nox and their cytotoxic effects in human vascular SMCs have not yet been investigated. Since 7-Kchol triggers a complex mode of cell death, characterized by an overproduction of ROS, associated with lipid peroxidation, oxidative DNA damage (37), and typical features of apoptosis (1, 12), the question arises as to whether the oxidant injury generated by 7-Kchol plays a role in the cytotoxic effects in vascular SMCs. Recently, Feng et al. (13) demonstrated that an excess of cellular cholesterol in macrophages induces free-cholesterol accumulation in the endoplasmic reticulum (ER) and triggers the unfolded protein response (UPR), which is the key signaling step in cholesterol-induced cell death. Signaling in the UPR emanates from the stressed ER and is characterized by several devastating intracellular events, including the depletion of the ER Ca^{2+} stores, the accumulation of misfolded proteins, and the activation of transcriptional factors involved in the downregulation of translation, the cell cycle, and the activation of cell death effectors. These findings led us to analyze the effects of 7-Kchol on intracellular ROS production and on the interplay between Nox-dependent production of ROS and the induction of ER stress and apoptosis in SMCs.

Our results show that 7-Kchol triggers the overproduction of Nox-4 and induces ER instability, leading to the activation of the UPR and proapoptotic signaling pathway and thus to SMC death. Nox-4 therefore appears to play a key role in this cascade of events; since when Nox-4 mRNA was silenced by using an RNA interference strategy, this completely prevented the deleterious effects caused by 7-Kchol in SMCs.

MATERIALS AND METHODS

Materials. A Lab-Tek Chamber Slide and Lab-Tek chambered cover-glass slides were from Nunc Int. (Naperville, Ill.). 7-α-Hydroxycholesterol was purchased from Steraloids. 7-Kchol, luminol, polyethylene glycol-linked superoxide dismutase (PEG-SOD), polyethylene glycol-linked catalase (PEG-catalase), diphenylene iodonium (DPI), and inhibitor cocktail were from Sigma (St. Louis, Mo.). 7-Ketocholesteryl-3-oleate was synthesized by one of the authors (M.S.). The degrees of purity of the oxysterols were confirmed to be 100% by gas chromatography-mass spectrometry. In most experiments, oxysterols were diluted in the culture medium at final concentration of 40 μg/ml (100 μM). 2′,7′-Dichlorofluorescin-diacetate DCFH-DA was from Acros-Organics (Geel, Belgium). The Nucleospin RNA II kit was from Macherey-Nagel (Hoerdt, France). TRIzol reagent, random hexamer, and Superscript II reverse transcriptase were purchased from Invitrogen (Cergy, France). Annexin V-fluorescein isothiocyanate (FITC), propidium iodide (PI), Z-VAD-fmk, mouse anti-GRP-78/Bip, anti-Bcl-2, anti-Bax, anti-calnexin, and anti-actin monoclonal antibodies (MAbs) were from Becton Dickinson (Le Pont de Claix, France), and mouse anti-CHOP/GADD153 MAb was from Tebu-Bio (Le Perray en Yvelines, France). Mouse anti-c-jun/AP-1 (Ab3) and rabbit anti-c-jun phospho-specific Ser^{73}, anti-SAPK/JNK, anti-SAPK/JNK phospho-specific Thr^{183} and Tyr^{185} and anthra[1,9-*cd*]pyrazol-6(2*H*)-one1,9-pyrazoloanthrone SAPK Inhibitor II (SP600125) were from Calbiochem (La Jolla, Calif.). Goat anti-IRE-1α was from Santa Cruz Biotechnology. Secondary antibodies were from Jackson Immunoresearch (West Baltimore Pike, Pa.). Hyperfilm MP, ECL, and alkaline phosphatase reagents were from Amersham Life Sciences (Arlington Heights, Ill.) and Bio-Rad. Fluo-3/AM was from VWR International (Fontenay s/s Bois, France). TransMessenger Transfection Reagent was from Qiagen (Courtaboeuf, France).

Cell culture. Human aortic SMCs (Cambrex, San Diego, Calif.) were grown in SmGM-2 SingleQuots medium supplemented with 5% fetal calf serum, as recommended by the manufacturer. The human monocytic cell line THP-1 was purchased from the American Type Culture Collection, and these cells were grown in RPMI 1640 containing 10% fetal calf serum, 2 mM L-glutamine, antibiotics, and 0.05 mM β-mercaptoethanol.

Immunoblot analysis. A rabbit anti-human-Nox-4 antibody was raised against the ^{88}KVPSRRTRRLLDKSR^{102} peptide synthesized by Neosystem (Strasbourg, France). Immunoglobulins were purified by being passed through a protein A-Sepharose column (0.9 by 4 cm) equilibrated in phosphate-buffered saline (PBS), eluted with 0.1 M glycine (pH 3.3). Samples were collected in tubes containing 50 μl of 2 M Tris (pH 11), dialyzed against PBS overnight at 4°C, and then concentrated. SMCs were cultured for various lengths of time with 40 μg of 7-Kchol, 7-α-hydroxycholesterol, or 7-ketocholesteryl-3-oleate/ml. Cells were rinsed, scraped, and collected in ice-cold PBS containing a cocktail of inhibitors. The protein concentration was measured by Bio-Rad assay with bovine serum albumin as a standard. Equal amounts of cell protein extract (25 μg) were subjected to sodium dodecyl sulfate-polyacrylamide gel electrophoresis (SDS-PAGE) on a 7 or 10% polyacrylamide gel. After being transferred onto nitrocellulose, membranes were blotted with the following primary antibodies diluted in Tris-buffered saline containing 0.1% Tween: rabbit anti-human Nox-4 (dilution 1/200), anti-c-jun phospho-specific Ser^{73}(dilution 1/2,000), anti-JNK (dilution 1/1,000), anti-JNK phospho-specific Thr^{183} and Tyr^{185} (dilution 1/5,000), mouse anti-CHOP/GADD153 (dilution 1/250), anti-GRP78/Bip (dilution 1/100), anti-Bax (dilution 1/300), anti-c-jun/AP-1 (dilution 1/1,000), and anti-Bcl-2 (dilution 1/100) MAbs and goat anti-IRE-1α antibody (dilution 1/200). After a rinsing step, the membranes were incubated with an appropriate secondary antibody (peroxidase-conjugated goat anti-rabbit, peroxidase-conjugated rabbit anti-goat, or peroxidase-conjugated sheep anti-mouse immunoglobulin G [IgG], dilution 1/20,000; alkaline phosphatase-conjugated goat anti-mouse and alkaline phosphatase-conjugated goat anti-rabbit IgG, dilution 1/5,000). The membranes were then washed in Tris-buffered saline–0.1% Tween, and proteins were detected by a chemiluminescence method or by using alkaline phosphatase. The blots were probed with a mouse anti-human actin MAb to confirm that they had been loaded equally. Bands were scanned with an HP Scanjet 5500, and the relative protein contents were determined by densitometric analysis.

Quantitative real-time RT-PCR analysis. Total RNA were extracted from SMCs by using TRIzol reagent or the Nucleospin RNA II kit according to the manufacturer's instructions. Equal amounts of total RNA were reverse transcribed by using a random hexamer and Superscript II reverse transcriptase. All of the samples for comparison were reverse transcribed from the same reverse transcription (RT) mixture. Expression levels of human Nox-1, Nox-4, Nox-5, and housekeeping α-actin mRNAs were determined by using the specific primer as follows: forward Nox-1 (5′-GTACAAATTCCAGTGTGCAGACCAC-3′) and reverse Nox-1 (5′-CAGACTGGAATATCGGTGACAGCA-3′), forward Nox-4 (5′-CTCAGCGGAATCAATCAGCTGTG-3′) and reverse Nox-4 (5′-AGAGGAACACGACAATCAGCCTTAG-3), forward Nox-5 (5′-ATCAAGCGGCCCCCTTTTTTTCAC3′) and reverse Nox-5 (5′-CTCATTGTCACACTCCTCGACAGC-3′), and forward α-actin (5′-GCAGCCCAGCCAGCACTGTCAGG-3′) and reverse α-actin (5′-AGCCCAGAGCCATTGTCACACACCAA-3′). The specificity of the products was demonstrated for each fragment by a melting curve analysis and gel electrophoresis. The QuantiTect SYBR Green PCR Master Mix (Qiagen) and the ABI Prism 7700 sequence detection system (Applied Biosystems) were used to detect the real-time quantitative PCR products of reverse-transcribed cDNA samples according to the manufacturer's instructions. The incubation conditions were as follows: 95°C for 15 min, followed by 40 cycles of 15 s at 94°C, annealing for 30 s, at 60°C, and extension for 30 s at 72°C. PCRs for each sample were done in triplicate for both the target genes and the α-actin control. mRNA expression was quantified by relating the PCR threshold cycle obtained from samples to a cDNA standard curve. For α-actin, the PCR threshold cycle was related to the number of SMCs that had been extracted. The normalized amount of Nox mRNAs was obtained by dividing the averaged sample value by the averaged α-actin value.

siRNA and cell transfection. Experiments were carried out with specific HPP 2-dT 3′ overhang small interfering RNA (siRNAs; Xeragon-Qiagen), designed by selecting a cDNA target region from Nox-4 (5′-AAACCGGCAGGAGUUUACCCAG-3′) located 768 bp from the start codon, and specific HPP Grade dXdY siRNA, designed by selecting a cDNA target region from IRE-1 (5′-CUGCCCGGCCUCGGGAUUUUU-3′) located 135 bp from the start codon. Scrambled siRNA (nonhomologous to the human genome, 5′-AACCAGCAAGGUGUAUCGCCAC-3′) was used as a control. To achieve optimal transfection efficiency, various parameters, including the amounts of transfection reagent, RNA, and TransMessenger-RNA complexes, the cell density, and the length of

exposure of cells to TransMessenger-RNA complexes, were optimized. At 24 h before transfection, SMCs were transferred onto six-well plates (5×10^5 cells per well) and transfected with 0.8 μg of each siRNA duplex by using TransMessenger transfection reagent for 4 h in medium devoid of serum and antibiotics. This procedure did not affect cell viability. SMCs were then washed once with PBS and grown in complete medium. Gene silencing was monitored after incubation for 24 h.

Transient-transfection and luciferase reporter assay. Human monocytic THP-1 cells (7×10^6 to 9×10^6 cells) were transfected by electroporation with pAP-1-Luc or $p(\kappa B)_3$ IFN-Luc plasmids (luciferase *cis*-reporter system containing AP-1 and NF-κB enhancer elements, respectively). Electric pulsing (275 V and 955 μF) was applied in the Bio-Rad Gene Pulser. Cells were placed on ice for 15 min and then seeded at 5×10^5 cells/well in six-well dishes. An empty luciferase plasmid, pLuc-MCS, was used as a control. After transfection, the cells were cultured for 48 h and then treated with 100 ng of TNF-α/ml or with various concentrations of 7-Kchol for a further 4 h. The cells were harvested, and the luciferase activities were measured by using a luminometer according to the manufacturer's instructions (Promega). All experiments were conducted in triplicate.

Confocal laser-scanning microscopy. (i) Indirect immunofluorescence studies. For indirect immunofluorescence, SMCs (5×10^4 per well) were fixed and permeabilized with cold methanol for 8 min and then incubated with rabbit anti-Nox-4 antibody (1/50) for 30 min at room temperature. After being rinsed with PBS, samples were incubated with an $Alexa_{568}$-conjugated affinity-purified goat anti-rabbit IgG (1/250) for 30 min. Samples were then incubated with a mouse anti-calnexin MAb (1/100) for 1 h. After two rinses with PBS, cells were incubated for 30 min with $Alexa_{488}$-conjugated affinity-purified goat anti-mouse IgG (1/250). After extensive rinsing, glass cover slides were mounted and examined by using a confocal laser-scanning microscope (CLSM-510-META; Zeiss, Mannheim, Germany) equipped with epifluorescent optics (×63 NA 1.3 oil-immersion objective lens). Simultaneous two-channel recording was performed with a pinhole size of 90 μm by using excitation wavelengths of 488 and 588 nm, a 510/580 double dichroic mirror, and a 515-to-545 band-pass FITC filter, together with a 590-nm long-pass filter. Double-labeled cells were analyzed separately to avoid leakage from one channel to another. Unstained controls were prepared by omitting the primary antibody. Preincubation of the Nox-4 antibody with the synthetic peptide (10 μg/ml) used for immunization resulted in undetectable signals, demonstrating the specificity of the antibody. The colocalization of the two antibodies was analyzed by using the colocalization Zeiss LSM5 Image Browser software.

(ii) Measurement of ROS generation by intact cells. The intracellular production of ROS was measured by confocal laser-scanning microscopy with 2′,7′-dichlorofluorescin-diacetate (DCFH-DA). SMCs plated on Lab-Tek chambered cover-glass slides (5×10^4 per well) were preincubated with or without oxysterols (40 μg/ml) for 16 h and were then loaded with 50 μM DCFH-DA for 20 min. DCFH-DA diffuses into cells, where it is hydrolyzed into 2′,7′-dichlorofluorescin (DCFH). Nonfluorescent intracellular DCFH is oxidized to form highly fluorescent dichlorofluorescein (DCF) by H_2O_2 derived from the dismutation of $O_2^{\cdot -}$. After excitation at 488 nm, the green fluorescence of DCF was measured on living cells by using the confocal microscope equipped with a cell culture chamber. When used, DPI (20 μM) was added 10 min before the DCFH-DA.

(iii) Measurement of intracellular Ca^{2+}. SMCs were seeded at 7.5×10^4 cells/ml onto Lab-Tek chambered cover glass slides. SMCs were loaded with 5 μM Fluo-3/AM (1 h, 37°C) in Hanks balanced salt solution, washed twice with the same buffer, and then examined by confocal microscopy. Fluo-3/AM, a fluorescent probe, is hydrolyzed by cellular esterases. The excitation wavelength was 506 nm, and the emission was monitored at 526 nm. Images were generated every 10 s for 20 min. Oxysterols (40 μg/ml) were added 3 min after the start of the experiment. The data reported are the fluorescence intensities (Zeiss LSM 5 Image Browser software), which reflect changes in cytosolic free Ca^{2+} concentration or $[Ca^{2+}]_i$.

Determination of apoptosis. (i) Cell detachment assay. Cells were seeded onto 12-well plates (10^6 cells per plate) and were treated with oxysterols (40 μg/ml) for 24 h. When used, the caspase inhibitor Z-VAD-fmk (200 μM) was added 1 h before this 24-h treatment. After exposure to the oxysterols, floating cells were recovered by centrifugation ($3,200 \times g$, 5 min) and counted. Adherent cells were rinsed three times with PBS, treated with trypsin, and counted.

(ii) Flow cytometry analysis. After counting, the floating and trypsinized attached cells were pooled. Samples were run on a Becton Dickinson FACScalibur (Immunocytometry Systems, San Jose, Calif.) equipped with a 15-mW, 488-nm argon laser and filter configuration for an FITC-PI dye combination. The quantitative determination of the percentage of cells undergoing apoptosis was performed by using the annexin V-FITC apoptosis detection kit according to the manufacturer's instructions.

The mitochondrial potential was measured by using 3,3′-dihexyloxacarbocyanine iodide ($DiOC_6$, 40 nM final concentration, 15 min, 37°C). $DiOC_6$ mitochondrial potential-related fluorescence was immediately recorded by flow cytometry.

ROS production assay. ROS production was measured by the peroxidase-dependent luminol-enhanced chemiluminescence assay using the Luminometer FluoStar counter (LBG). Untransfected or siRNA-transfected SMCs (5×10^5 cells per well in 12-well plates) were exposed to 40 μg of oxysterols/ml for 16 h. Measurements were performed for 30 min in Hanks balanced salt solution supplemented with 20 U of peroxidase/ml. The preincubation times were 5 min for the combination of PEG-SOD (10 μg/ml) plus PEG-catalase (10 U/ml) and 30 min for DPI (20 μM).

Statistical analysis. Results are expressed as means ± the standard deviations (SD) from triplicate determinations from three to four separate experiments for each set of conditions tested. Significant differences between groups were analyzed by using an unpaired Student *t* test. A *P* value of <0.05 was considered significant.

Accession numbers. The GenBank accession numbers were as follows: human Nox-1 (AJ438989), Nox-4 (AF254621), and Nox-5 (AF317889).

RESULTS

7-Kchol stimulates the expression of Nox-4 in SMCs. We first investigated the effects of 7-Kchol on the regulation of Nox mRNA expression in SMCs. The results from real-time PCR revealed that SMCs expressed the NAD(P)H homologues, Nox-1, Nox-4, and Nox-5 (Fig. 1A), whereas Nox-2 and Nox-3 mRNAs were not detected under our experimental conditions. 7-Kchol did not alter the basal levels of Nox-1 and Nox-5 mRNAs in SMCs but significantly increased the level of Nox-4 mRNA in a dose- and time-dependent manner (by ~3-fold, $P < 0.01$) (Fig. 1A and B). In contrast, the level of Nox-4 mRNA expression in SMCs was not affected by 7-α-hydroxycholesterol (Fig. 1B). The esterification of oxysterols has been shown to reduce their cytotoxic and oxidative capacities, thereby delaying the progression of atherosclerosis (9, 37). We therefore investigated whether the chemically synthesized ester of 7-Kchol, the 7-ketocholesteryl-3-oleate, affected the expression of Nox-4. 7-Ketocholesteryl-3-oleate was mainly incorporated into the plasma membrane (data not shown). We found that it failed to exert any regulatory action on Nox-4 mRNA level regardless of the time and the concentration used (Fig. 1B).

An antibody raised against a customized peptide of human Nox-4 protein was generated to find out whether the 7-Kchol-dependent overexpression of Nox-4 mRNA in SMCs could also be detected at the protein level. Western blot analyses, with the anti-Nox-4 antibody generated, revealed a single protein band with an apparent molecular mass of ~70 kDa. This was not detected when the membrane had been preincubated with an excess of the synthetic peptide used for immunization (data not shown). SMCs were then incubated with or without 40 μg of 100 μM 7-Kchol, 7-α-hydroxycholesterol, or 7-ketocholesteryl-3-oleate/ml for 8 and 16 h. A significant increase in the relative amount of Nox-4 protein occurred only with 7-Kchol (Fig. 1C).

These findings demonstrate that 7-Kchol specifically induces the overexpression of Nox-4 at both the mRNA and protein levels in SMCs.

7-Kchol stimulates ROS production in SMCs. The predominant role of oxidative stress in atherosclerosis and the close relationship between clinical risk factors and NAD(P)H oxi-

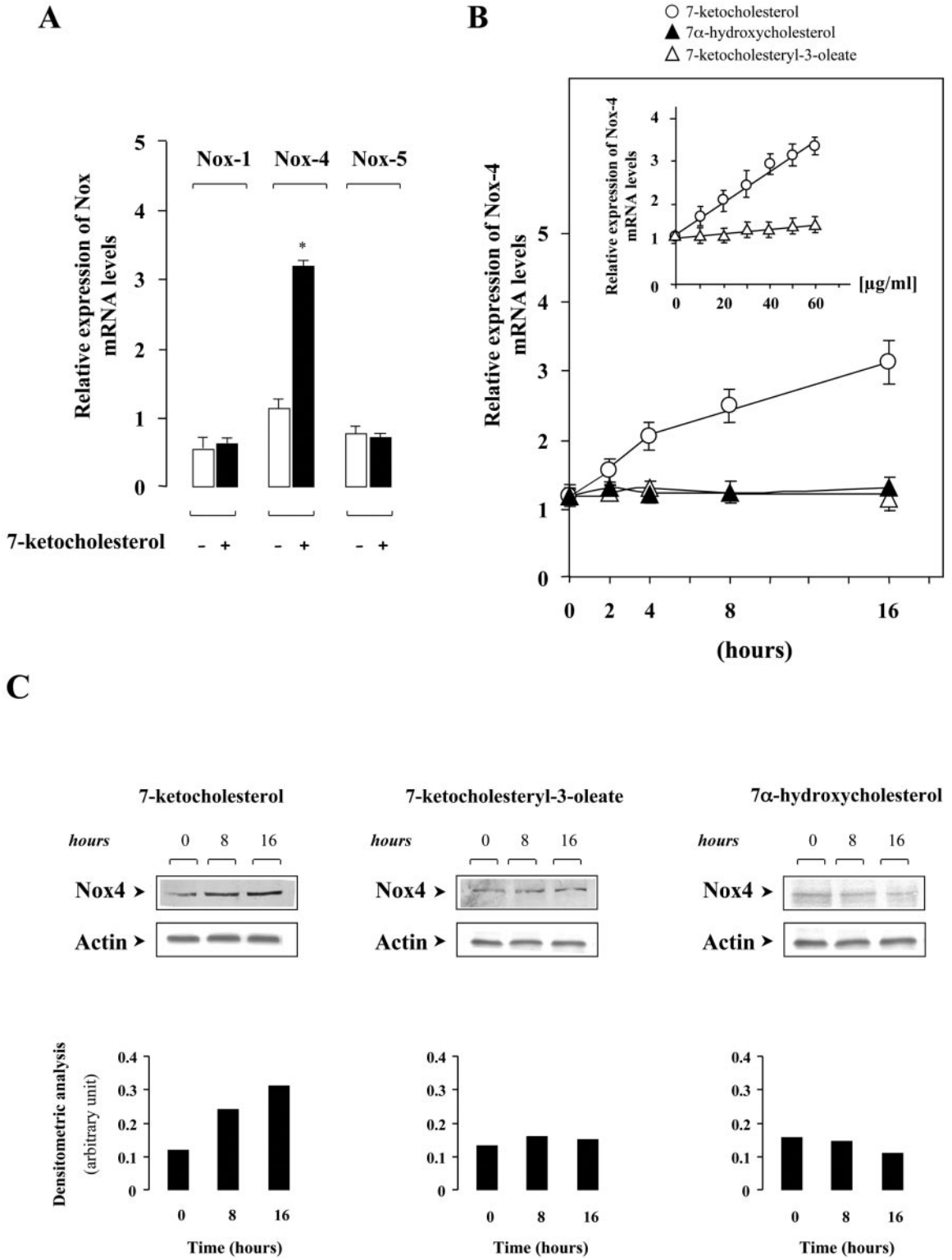

FIG. 1. 7-Kchol stimulates Nox-4 mRNA expression in SMCs. (A) Subconfluent SMCs were incubated with 0 or 40 μg of 7-Kchol/ml for 16 h. Nox mRNA expression levels were quantified by real-time RT-PCR. The bars, expressed as the relative expression of Nox versus α-actin mRNA levels, are means ± the SD from three independent experiments. ✻, $P < 0.01$. (B) Subconfluent SMCs were treated with oxysterols (40 μg/ml) for various times and concentrations (inset), and the relative expression of Nox-4 mRNA was determined by real-time RT-PCR. (C) Western blot analysis, with an anti-Nox-4 antibody and an anti-α-actin antibody, were performed on untreated (time zero) and oxysterol-treated SMCs for 8 and 16 h. The bars correspond to the densitometric value of Nox-4 over α-actin, and results are representative of three separate experiments.

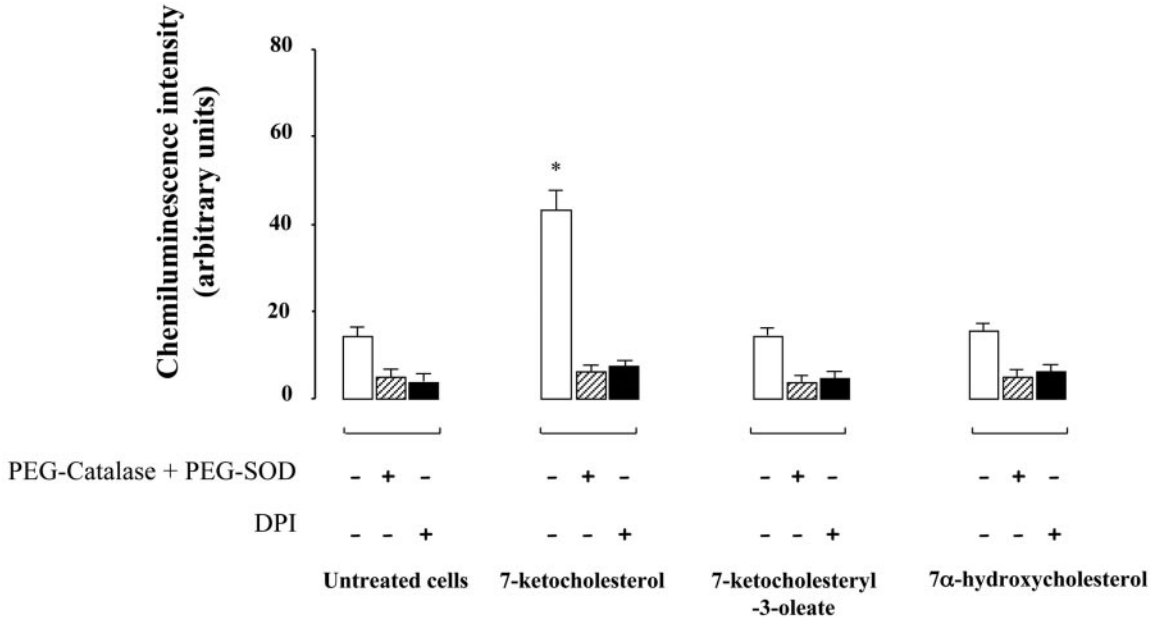

FIG. 2. 7-Kchol stimulates the intracellular production of ROS in SMCs. Cells were incubated with or without oxysterols (40 μg/ml) for 16 h, and ROS production was measured by chemiluminescence assay. Preincubation times were 5 min for the combination of PEG-SOD (10 μg/ml) plus PEG-catalase (10 U/ml) and 30 min for DPI (20 μM), respectively. The values, expressed as the relative chemiluminescence intensity, are means ± the SD of triplicate measurements from three separate experiments. ✱, $P < 0.01$.

dase-dependent production of ROS in human arteries (17) prompted us to try to find out whether the overexpression of Nox-4 induced by 7-Kchol contributes to the increased ROS production by SMCs. SMCs were incubated with or without 40 μg of 7-Kchol, 7-ketocholesteryl-3-oleate, or 7-α-hydroxycholesterol/ml for 16 h, and ROS production was then assayed by using a luminol-enhanced chemiluminescence assay. 7-Kchol caused a significant increase in chemiluminescence intensity that was inhibited by adding a combination of cell-permeable PEG-SOD and PEG-catalase (Fig. 2). These findings suggested that light emission resulted from the production of superoxide ($O_2^{\cdot -}$) and hydrogen peroxide (H_2O_2). The control, unmodified SOD, and catalase enzymes failed to inhibit chemiluminescence (data not shown). In addition, the 7-Kchol-dependent production of ROS was reduced by the flavoprotein inhibitor DPI, suggesting that ROS production depends on the activity of NAD(P)H oxidase. Furthermore, 7-α-hydroxycholesterol or 7-ketocholesteryl-3-oleate did not affect the basal production of ROS in SMCs (Fig. 2). Substantial cellular ROS production was also detected in SMCs by using the cell-permeable DCFH-DA reagent. Cells were incubated with 7-Kchol for 16 h before the addition of DCFH-DA, and the intracellular ROS production was assessed by the oxidation of DCFH into the highly fluorescent DCF, which was monitored by confocal microscopy for 30 min in living cells. Untreated SMCs weakly oxidized DCFH (Fig. 3Aa and b). Exposure to 7-Kchol for 16 h increased fluorescent-DCF production in the cytoplasm of SMCs (Fig. 3Ac and d). As a control, DPI significantly decreased the 7-Kchol-induced fluorescence intensity (Fig. 3Ae and f). Furthermore, 7-α-hydroxycholesterol and 7-ketocholesteryl-3-oleate had no effect on the fluorescence intensity (data not shown), indicating that 7-Kchol specifically induced the production of intracellular ROS in SMCs.

The intracellular localization of Nox-4 protein in SMCs was then analyzed by indirect immunofluorescence with the Nox-4 antibody (Fig. 3B). Confocal microscopy analyses revealed that the immunostaining was concentrated in both the paranuclear and nuclear regions of SMCs. The specificity of the Nox-4 antiserum used was confirmed by the fact that no staining was detected when the primary antibody was preincubated with the synthetic peptide used for the immunizations (Fig. 3B, upper panels) when the primary antibody was omitted or replaced by preimmune rabbit IgG (data not shown). Double immunofluorescence studies also revealed that Nox-4 colocalized with the ER marker calnexin, indicating that Nox-4 was located in the ER (Fig. 3B, lower panels).

Nox-4 is responsible for the 7-Kchol-dependent production of ROS. Experiments with specific siRNA duplexes to silence Nox-4 expression in SMCs were performed to find out whether the 7-Kchol-dependent production of ROS is due, at least in part, to Nox-4 overexpression. A first set of experiments was undertaken to determine whether Nox-4 siRNAs specifically reduced Nox-4 mRNA expression without modifying the expression of other Nox mRNA species. SMCs were transfected with specific Nox-4 or scrambled siRNAs, and the expression of various Nox mRNAs was quantified by real-time PCR analysis before and after incubation of the cells with 7-Kchol for 16 h (Fig. 4A). Scrambled siRNA did not significantly alter the basal level of expression of Nox mRNA compared to nontransfected cells (see Fig. 1A and 4A). SMCs transfected with the specific Nox-4 siRNA reduced the basal level of Nox-4 mRNA by 80% compared to that of scrambled siRNA-transfected

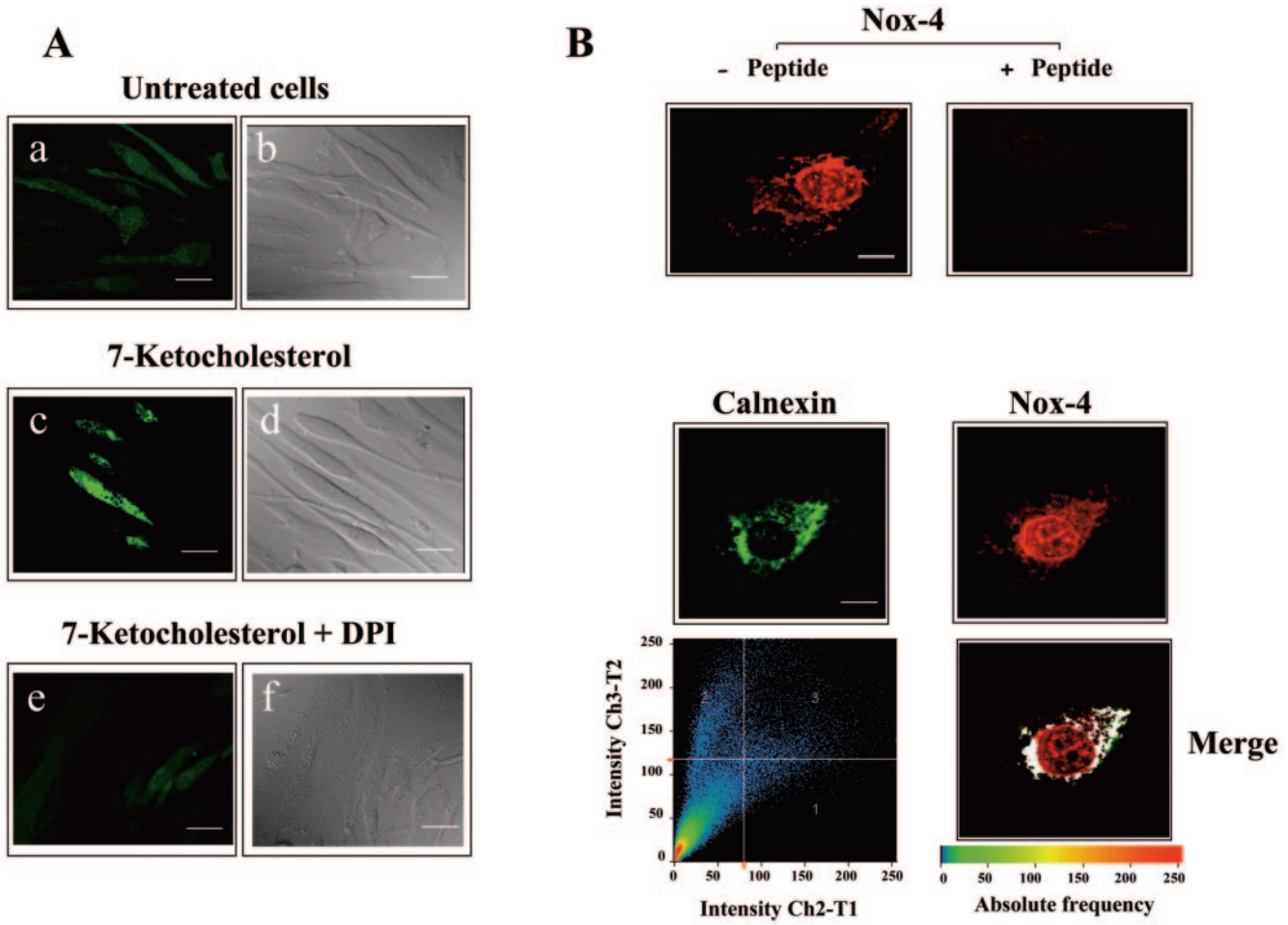

FIG. 3. ROS produced by 7-Kchol and Nox-4 exhibit paranuclear and nuclear localization in SMCs. (A) Cells were incubated in the presence or absence of 40 μg of 7-Kchol/ml for 16 h and then with the peroxide-sensitive fluorophore DCFH-DA for 20 min. DPI (20 μM) was added 10 min before and during DCFH-DA loading. Images were obtained by confocal laser-scanning microscopy. Fluorescence labeling (a, c, and e) and phase-contrast images (b, d, and f) are shown. Bars, 20 μm. (B) In the upper panels, SMCs were processed for indirect immunofluorescence with the anti-Nox-4 polyclonal antibody with or without preincubation with 10 μg of synthetic peptide/ml. Bars, 15 μm. In the lower panels, SMCs were processed for double indirect immunofluorescence with a mouse anticalnexin MAb (green) and the anti-Nox-4 polyclonal antibody (red). Note the colocalization of the proteins (Merge) in the paranuclear region of SMCs. Bar, 15 μm.

SMCs (Fig. 4A). The inhibitory effect on Nox-4 mRNA expression appeared to be specific, since the mRNA levels of Nox-1 and Nox-5 were not affected by transfection with Nox-4 siRNA. Nox-4 silencing decreased the 7-Kchol-dependent induction of Nox-4 mRNA expression by 83% compared to scrambled siRNA-transfected SMCs (Fig. 4A). Overall, these findings demonstrate the specificity of 7-Kchol toward Nox-4 mRNA expression in SMCs.

To further validate the silencing effect, the amount of Nox-4 protein in scrambled siRNA- or Nox-4 siRNA-transfected SMCs incubated with or without 7-Kchol for 16 h was analyzed by Western blotting with the Nox-4 antibody. Consistent with the loss of Nox-4 mRNA, the amount of Nox-4 protein detected was dramatically lower in Nox-4 siRNA-transfected SMCs than in scrambled siRNA-transfected SMCs (Fig. 4B). Densitometric analyses of the amount of Nox-4, corrected for the amount of α-actin used as an internal standard, showed that 7-Kchol significantly enhanced the amount of Nox-4 protein in scrambled siRNA-transfected SMCs but not in Nox-4 siRNA-transfected SMCs (Fig. 4B).

To find out whether Nox-4 silencing can also influence the 7-Kchol-generated production of ROS in SMCs, chemiluminescence analysis was used to assay ROS production in both Nox-4 siRNA- and scrambled siRNA-transfected SMCs. The stimulation of ROS by 7-Kchol, which was in the same range in scrambled siRNA-transfected and in nontransfected SMCs (Fig. 4C and 2), was inhibited by adding PEG-SOD plus PEG-catalase, but 7-Kchol failed to generate the production of ROS in Nox-4 siRNA-transfected SMCs (Fig. 4C). These findings demonstrate that Nox-4 plays a crucial role in the increase in 7-Kchol-induced production of ROS by SMCs.

Nox-4 silencing prevents the 7-Kchol-induced death of SMCs. Since 7-Kchol stimulates Nox-4 expression and ROS-associated production, we investigated the role of Nox-4 in 7-Kchol-induced cell death in SMCs. The effect on cell death of incubating SMCs for 24 h with 7-Kchol was analyzed in

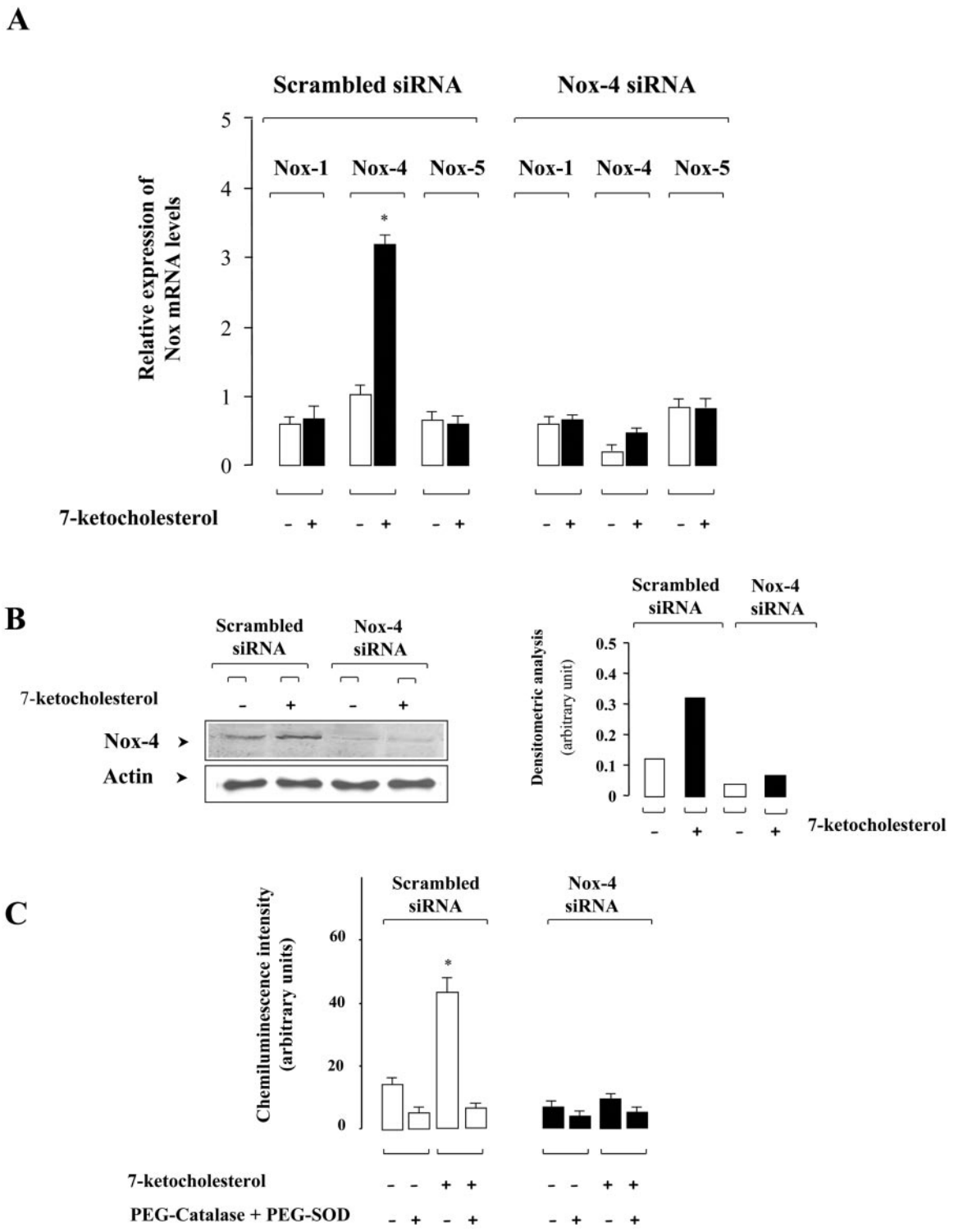

FIG. 4. Silencing of Nox-4 expression by RNA interference in SMCs. (A) Cells were transfected with scrambled siRNA or Nox-4 siRNA duplexes. After incubation for 24 h in complete medium, SMCs were treated with 0 or 40 μg of 7-Kchol/ml for 16 h. Nox mRNA expression levels were then determined by real-time RT-PCR. Bars, indicating the relative expression of Nox versus α-actin mRNA levels, are means ± the SD from three independent experiments. ✻, $P < 0.01$. (B) SMCs transfected with scrambled or Nox-4 siRNAs were treated with 0 or 40 μg of 7-Kchol/ml for 16 h. The expression of Nox-4 was detected by Western blot analysis with the anti-Nox-4 antibody. The bars represent the mean densitometric value of Nox-4 over α-actin from three separate experiments for each of the experimental conditions tested. (C) ROS production (chemiluminescence assay) was measured on SMCs transfected with scrambled or Nox-4 siRNAs incubated with 0 or 40 μg of 7-Kchol/ml for 16 h. A combination of PEG-SOD (10 μg/ml) and PEG-catalase (10 U/ml) was added 5 min before the chemiluminescence assay. The chemiluminescence intensity values reported are means ± the SD from three separate experiments performed in triplicate. ✻, $P < 0.01$.

Nox-4 siRNA- and scrambled siRNA-transfected SMCs by using the annexin V-binding assay. The affinity of annexin V for the phosphatidylserine residues makes it possible to determine the percentage of apoptotic cells by flow cytometry (Fig. 5A and B). Apoptotic (annexin V^+/PI^-), necrotic (annexin V^+/PI^+), and damaged (annexin V^-/PI^+) cells were distinguished on the basis of a double labeling for annexin V-FITC and PI, a membrane-impermeable DNA stain. Untreated cells transfected with either scrambled or Nox-4 siRNAs showed a similar low pattern of fluorescent staining (Fig. 5B). 7-Kchol led to a dramatic increase in the percentage of apoptotic cells (35 to 40% of the total cell population) and, to a lesser extent, of necrotic cells (15% of the total cell population) and damaged cells (10 to 12% of the total cell population) in nontransfected (data not shown) and scrambled-siRNA transfected SMCs. In contrast, the number of apoptotic cells in 7-Kchol-treated Nox-4 siRNA-transfected SMCs was 75% lower than in 7-Kchol-treated scrambled siRNA-transfected SMCs.

We then investigated the involvement of caspases in the 7-Kchol-induced apoptotic process. The proportion of detached (floating) cells and attached cells in both cell populations was determined in the presence or absence of Z-VAD-fmk, a wide-spectrum caspase inhibitor (Fig. 5C). As expected, 7-Kchol significantly increased the fraction of floating cells in scrambled siRNA-transfected SMCs; this increase was almost completely prevented by Z-VAD-fmk (Fig. 5C). These findings confirm the involvement of caspases in 7-Kchol-induced apoptosis (30, 35). In contrast, 7-Kchol failed to induce cell detachment in Nox-4 siRNA-transfected SMCs (Fig. 5C), suggesting that the loss of Nox-4 expression usually conferred resistance to 7-Kchol cytotoxicity.

The question therefore arises as to whether the prevention of cell death due to the absence of Nox-4 expression was associated with impairment of the opening of the mitochondrial megachannels, resulting in the loss of the mitochondrial potential, a major event in the onset of apoptosis (15). Modification of mitochondrial potential was quantified by flow cytometry using $DiOC_6$ in both scrambled siRNA- and Nox-4 siRNA-transfected cells incubated with 7-Kchol for 24 h (Fig. 5D). The percentage of depolarized cells (characterized by low potential values) reached 60 to 65% in 7-Kchol-treated scrambled siRNA-transfected SMCs, whereas only a small percentage of depolarized cells was detected in 7-Kchol-treated Nox-4 siRNA-transfected SMCs. These findings demonstrate that Nox-4 is directly involved in the triggering of 7-Kchol-induced apoptosis in SMCs.

The UPR is activated in 7-Kchol-treated SMCs. The fact that Nox-4 was located in the ER from SMCs and that Nox-4 silencing prevented the increased ROS production and 7-Kchol-induced apoptosis led us to suggest that 7-Kchol may play a key role in the cellular responses elicited by ER stress and thereby participate in the UPR signaling pathway in SMCs. Depletion of luminal ER Ca^{2+} stores is thought to reflect ER stress which, under certain circumstances, can promote the induction of UPR (50). Previous studies have shown that ER Ca^{2+} pools can be modulated by incubating vascular SMCs with oxysterols other than 7-Kchol (2, 3). To find out whether 7-Kchol also had this effect on intracellular Ca^{2+} stores, SMCs were loaded for 1 h with the fluorescent Ca^{2+} Fluo-3/AM indicator, and fluorescent signals were recorded at 10-s intervals over 20 min (Fig. 6). Adding 7-Kchol caused a rapid change in the intracellular Ca^{2+} pool, with transient oscillations of cytosolic Ca^{2+}. This effect was not observed when SMCs were incubated with 7-ketocholesteryl-3-oleate (Fig. 6). However, 7-Kchol also generated similar transient oscillations of Ca^{2+} in Nox-4 siRNA-transfected SMCs (Fig. 6). These findings indicated that the very rapid induction of Ca^{2+} oscillations induced by 7-Kchol is not affected by Nox-4 silencing in SMCs (Fig. 6).

We then investigated the effects of 7-Kchol on the expression of the transcription factor CHOP/GADD153 (56) and the coordinately regulated chaperone GRP78/Bip (8), two hallmarks of the UPR pathway that culminate in the induction of ER stress. The expression of the antiapoptotic protein Bcl-2, whose promoter activity is inhibited by elevated CHOP expression (33), and the proapoptotic factor Bax, which increases the likelihood that vascular SMCs will undergo apoptosis (22) and contributes to ER stress-induced apoptosis (52), were also analyzed. CHOP expression, assessed by Western blot analysis, was markedly induced by 7-Kchol in nontransfected SMCs (data not shown) and scrambled siRNA-transfected SMCs but was barely detectable in 7-Kchol-treated Nox-4 siRNA-transfected SMCs (Fig. 7). The effects of 7-Kchol on the amounts of GRP78/Bip chaperone, antiapoptotic Blc-2 and proapoptotic Bax proteins were then analyzed by Western blotting. The amount of GRP78/Bip and Bax proteins increased, whereas the level of Bcl-2 dramatically decreased in scrambled siRNA-transfected SMCs incubated with 7-Kchol (Fig. 7). In contrast, 7-Kchol did not affect the amounts of these proteins in Nox-4 siRNA-transfected SMCs. These results demonstrate that Nox-4 plays a key role in the onset of programmed SMC death in response to 7-Kchol injury. The prevention of CHOP and GPR78/Bip overexpression by Nox-4 siRNA also suggested that Nox-4 may be part of an ER signaling pathway that is activated by 7-Kchol in SMCs.

Activation of the ER stress-dependent IRE-1/JNK/AP-1 pathway is required for 7-Kchol-induced Nox-4 expression. Among the adaptive signaling pathways triggered by ER stress, the c-Jun NH_2-terminal kinases (JNK) constitute a family of stress-activated protein kinases that regulate gene expression by modulating the transcriptional factor AP-1 and participate in deciding between apoptosis or survival responses. Upstream from JNK, ER stress activates the ER-transmembrane kinase IRE-1, one of the UPR sensors that controls both the survival and the apoptotic pathways (51). Its endoribonuclease activity on the transcription factor XBP-1 mRNA induces UPR genes, such as GRP78/Bip, GRP94, and calreticulin. Prolonged UPR activation leads to cell death in which IRE-1 exerts a proapoptotic function. Activated IRE-1 recruits cytosolic TNF receptor-associated factor 2 to activate apoptosis-signal-regulating kinase (ASK1), which in turn contributes to the sustained activation of JNK and leads cells to apoptosis (49).

We thought that 7-Kchol-induced ER stress might enhance the activation of the IRE-1/JNK/AP-1 signaling pathway, which could contribute to Nox-4 expression during ER stress. To validate this hypothesis, we first used Western blot analysis with phospho-specific anti-JNK and anti-c-jun antibodies to assay JNK activation in SMCs that had or had not been treated with 7-Kchol. Although the levels of total JNK and c-jun were not affected by 7-Kchol, the oxysterol did induce a progressive

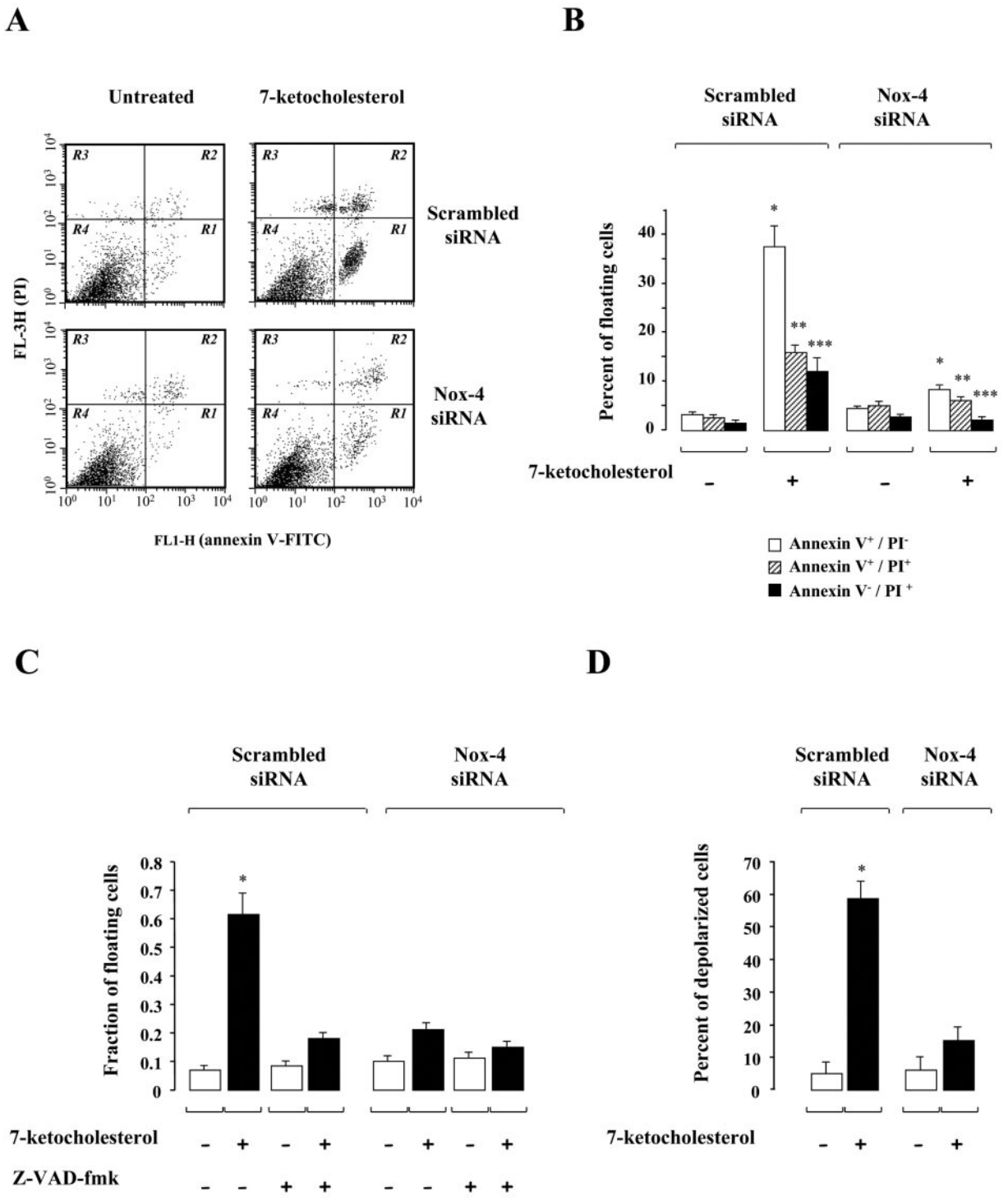

FIG. 5. Silencing of Nox-4 expression prevents 7-Kchol-induced apoptosis in SMCs. (A) Flow cytometry analyses were performed on scrambled siRNA- or Nox-4 siRNA-transfected SMCs incubated with 0 or 40 μg of 7-Kchol/ml for 24 h. The plots of annexin V versus PI fluorescence shown correspond to three independent experiments. R1, apoptotic cells (annexin V^+/PI^-); R2, necrotic cells (annexin V^+/PI^+); R3, damaged cells (annexin V^-/PI^+); R4, viable cells (annexin V^-/PI^-). (B) The bars represent the percentage of annexin V^+/PI^-, annexin V^+/PI^+, and annexin V^-/PI^+ cells after exposure to 40 μg of 7-Kchol/ml for 24 h. The values reported are means ± the SD of three separate experiments. ✻, $P < 0.001$; ✻✻, $P < 0.01$; ✻✻✻, $P < 0.05$ (versus −7 Kchol values for each experimental condition tested). (C) 7-Kchol-induced apoptosis is sensitive to the pan caspase inhibitor Z-VAD-fmk. The ratio of floating to attached cells was determined on scrambled siRNA- or Nox-4 siRNA-transfected SMCs that had or had not been exposed to 7-Kchol for 24 h and 200 μM pancaspase inhibitor Z-VAD-fmk. The values reported are means ± the SD of triplicate counts from four independent experiments. ✻, $P < 0.01$. (D) Percentage of depolarized cells characterized by loss of mitochondrial transmembrane potential. SMCs transfected with scrambled or Nox-4 siRNAs were incubated with 0 or 40 μg of 7-Kchol/ml for 24 h. The percentage of cells with low mitochondrial potential was quantified by flow cytometry with $DiOC_6$. The values reported are means ± the SD of four independent experiments. ✻, $P < 0.01$.

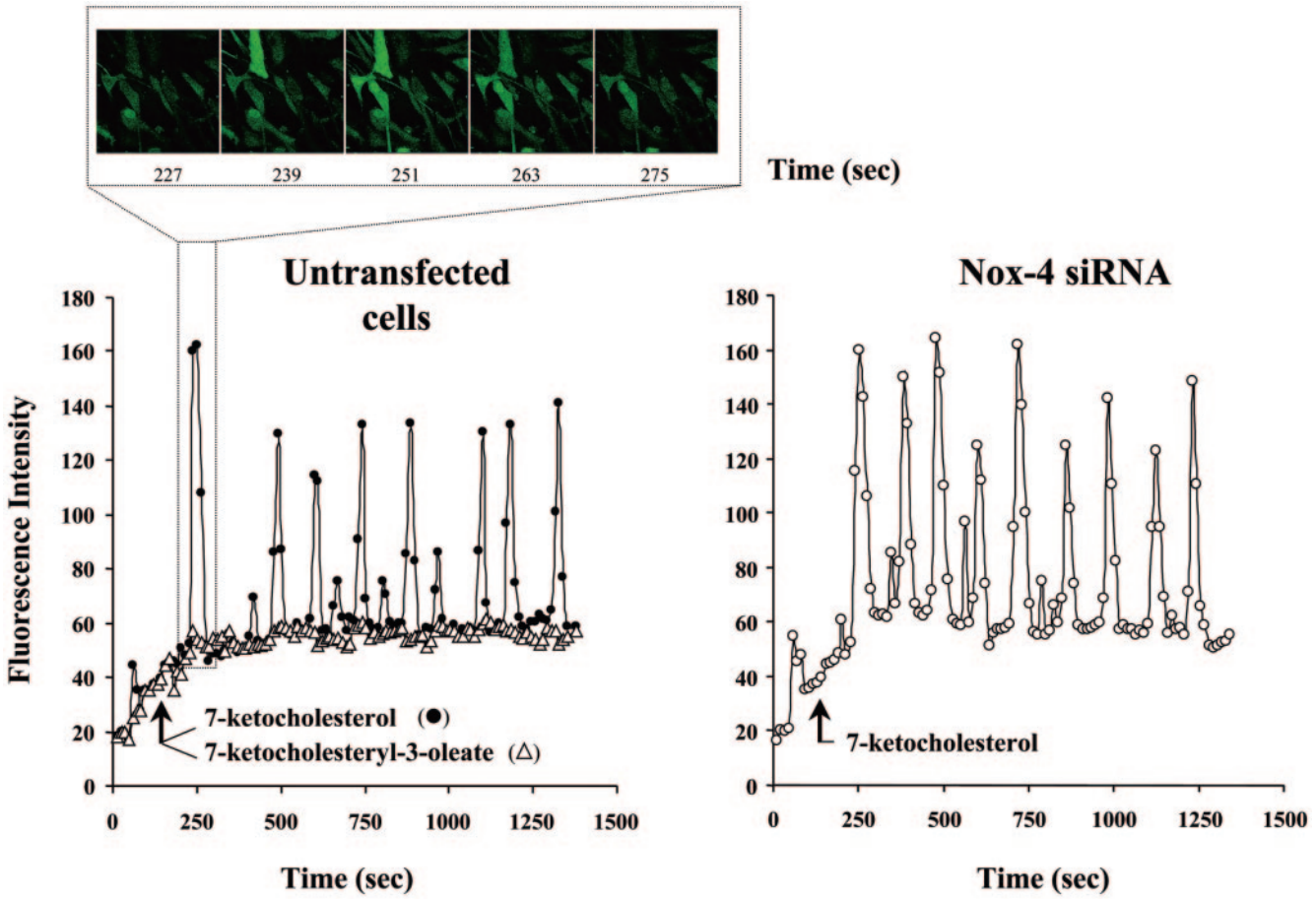

FIG. 6. 7-Kchol induces Ca^{2+} oscillations in SMCs. Untransfected and Nox-4 siRNA-transfected SMCs were loaded with Fluo-3/AM (5 μM, 1 h, 37°C) and placed in a culture chamber adapter to an inverted microscope. Then, 40 μg of 7-Kchol or 7-ketocholesteryl-3-oleate/ml were added 3 min after the start of the experiment. The images were generated by confocal microscopy every 10 s over a period of 20 min. The data are reported as the fluorescence intensity, reflecting changes in $[Ca^{2+}]_i$. The upper panel provides an illustration of real-time imaging generated by confocal microscopy.

increase in the level of JNK and c-jun phospho-proteins (Fig. 8A). Increased phosphorylation of c-jun is known to trigger partial activation of transcription factor AP-1. To find out whether 7-Kchol could modulate AP-1 activity, human monocytic THP-1 cells were transiently transfected with an AP-1 driven luciferase reporter gene and then exposed to various concentrations of 7-Kchol. It is still difficult to carry out transient-transfection studies in SMCs, and so the experiments were conducted on THP-1 cells, which readily overexpress such plasmids. 7-Kchol induced a dose-dependent increase in AP-1 transcriptional activity (Fig. 8B). NF-κB activation is known to be involved in regulating the ER-overload response, which is a pathway in the ER stress-induced signal transduction (38), and in downregulating the proapoptotic JNK pathway in other systems (21). For these reasons, we also tested the effect of 7-Kchol on NF-κB activity. THP-1 cells transiently transfected with a NF-κB promoter linked to a luciferase reporter gene construct were incubated with different concentrations of 7-Kchol. 7-Kchol failed to stimulate NF-κB transcriptional activity at any of the concentrations tested (Fig. 8B). In the controls, TNF-α (100 ng/ml), which is known to activate both AP-1 (7) and NF-κB (4), induced intense luciferase activity in THP-1 cells transfected with the two reporter constructs (Fig. 8B). These results indicate that 7-Kchol promotes the activation of AP-1 but not of NF-κB.

We next wanted to find out whether the JNK/AP-1 pathway activated by 7-Kchol could induce Nox-4 expression in SMCs. SMCs were therefore incubated with or without 7-Kchol for 16 h and in the presence or the absence of SP600125, a specific inhibitor of JNK activity. Real-time PCR experiments revealed that SP600125 decreased the 7-Kchol-stimulated expression of Nox-4 mRNA by 77%. Consistent with this, we also found that SP600125 completely prevented the increase in Nox-4 protein determined by Western blotting in 7-Kchol-treated SMCs (Fig. 8D). Furthermore, SP600125 also prevented the 7-Kchol induction of CHOP and GRP78/Bip proteins (Fig. 8D). Overall, these findings suggest that the activation of the ER-stress-dependent JNK/AP-1 pathway induced by 7-Kchol is involved in the upregulation of Nox-4 expression.

To further clarify the process by which ER stress is induced by 7-Kchol, SMCs were transfected with specific siRNA duplexes to silence IRE-1 acting further upstream on the JNK signaling pathway. Western blotting with a specific anti-IRE-1α antibody revealed two protein bands in both scram-

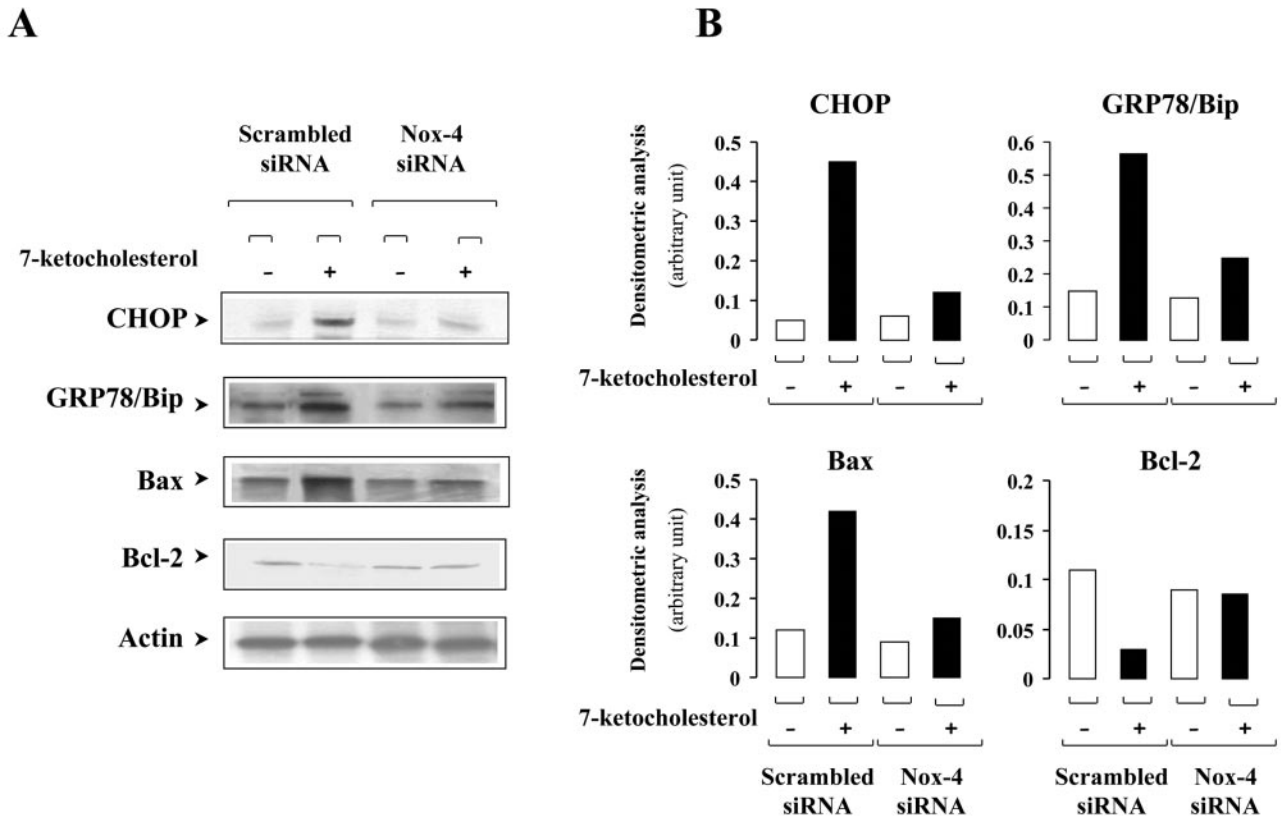

FIG. 7. Silencing of Nox-4 expression prevents the UPR induced by 7-Kchol. (A) Lysates of SMCs transfected with scrambled or Nox-4 siRNAs incubated with or without 40 μg of 7-Kchol/ml for 24 h were immunoblotted for CHOP/GADD 153, GRP78/Bip, and proapoptotic Bax and for antiapoptotic Bcl-2 and α-actin. (B) The relative protein content of samples was determined with an anti-α-actin antibody. The bars represent the densitometric value for each experimental condition and are representative of three separate experiments.

bled siRNA- and IRE-1-transfected cells (Fig. 9). As also shown in Fig. 9, scrambled siRNA-transfected cells incubated with 7-Kchol exhibited more of the shifted band with a higher molecular weight corresponding to the autophosphorylated, activated form of IRE-1 (51). In contrast, the relative IRE-1 protein content was markedly lower in untreated and 7-Kchol-treated IRE-1 siRNA-transfected SMCs than in scrambled siRNA-transfected SMCs (Fig. 9). 7-Kchol treatment, which increases the amount of Nox-4 protein, also enhanced the amount of JNK-P in scrambled siRNA-transfected SMCs but had no effect in IRE-1 siRNA-transfected SMCs (Fig. 9). In addition, silencing of IRE-1 prevented the 7-Kchol-induced cell death observed in Nox-4 siRNA-transfected SMCs (data not shown). These data indicate that the 7-Kchol-induced expression of Nox-4 that triggers SMC death occurs via the ER stress IRE-1/JNK/AP-1 signaling pathway.

DISCUSSION

Apoptosis is considered as an essential pathophysiological phenomenon in atherosclerosis (27), and it is agreed that the presence of apoptotic SMCs plays a key role in plaque rupture. The apoptosis of vascular SMCs has a dramatic impact on the development of atherosclerosis, and so it is useful to identify the substances that induce apoptotic processes in these cells and to elucidate their intracellular signaling pathways in the hope of being able to apply this knowledge in clinical practice. One of these substances, 7-Kchol, must play an important role, since high levels of this oxysterol are often detected in atherosclerotic plaques (9) and can induce apoptosis in vascular SMCs (30).

We report here for the first time that Nox-4 protein plays a key role in the overproduction of ROS and in the control of apoptosis induced by 7-Kchol in cultured human SMCs. It is noteworthy that, among the three different Nox proteins identified in SMCs, the Nox-4 protein is the only one to be upregulated by 7-Kchol and that the Nox-4 silencing experiments show that it appears to be responsible for 7-Kchol-induced production of ROS. The effect of 7-Kchol appears to be rather specific, since 7-α-hydroxycholesterol and 7-ketocholesteryl-3-oleate, which have no cytotoxic effect within SMCs, failed to exert any regulatory effect on either Nox-4 expression or ROS production. These findings are consistent with the fact that esterification of oxysterols delays the progression of atherosclerosis by reducing the oxidative potential and cytotoxicity of these substances (9, 37). In the present study, we used a 7-Kchol concentration of 40 μg/ml, which is ~25-fold higher than levels found in human plasma after a fat-rich meal. However, this concentration is compatible with the high levels of oxidized lipids accumulated in advanced human atherosclerotic plaque and is close to the levels found in the plasma of

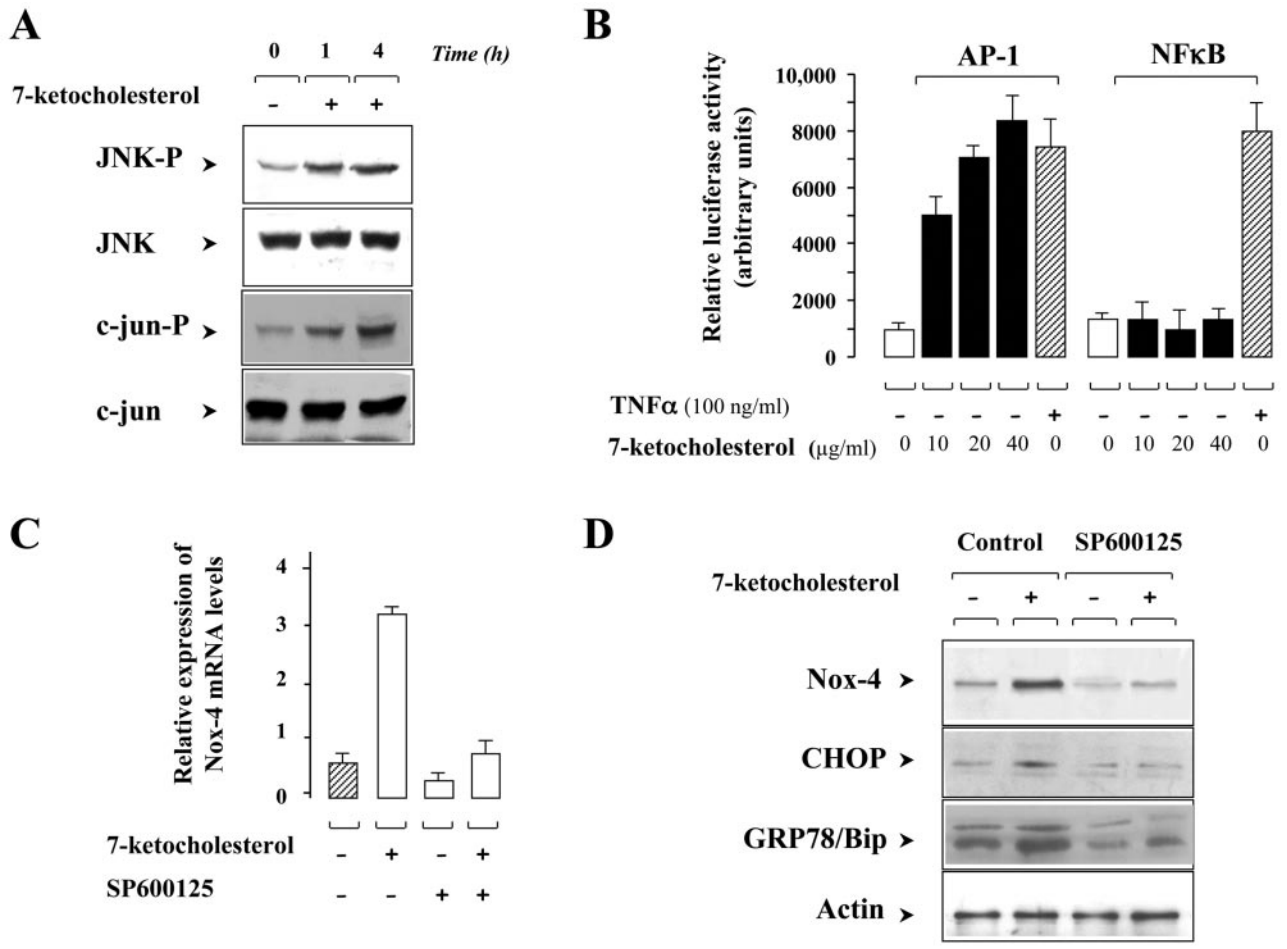

FIG. 8. ER stress-dependent JNK activation is required for 7-Kchol-induced Nox-4 overexpression. (A) Western blot analyses with antibodies directed against anti-JNK phospho-specific Thr^{183} and Tyr^{185}, anti- JNK, anti-c-jun phospho-specific Ser^{73}, and anti-c-jun, were performed on untreated (time zero) and 7-Kchol-treated (times 1 and 4 h) SMCs. (B) Human monocytic THP-1 cells were transiently transfected with plasmids expressing the indicated luciferase *cis*-reporters (NF-κB or AP-1). Luciferase activities were measured after exposure for 4 h to the indicated concentrations of 7-Kchol. TNF-α (100 ng/ml) was used as a positive control. The bars are means ± the SD of relative luminescence intensity values from three separate experiments performed in triplicate. (C) SMCs were treated with 40 μg of 7-Kchol/ml for 16 h with or without 40 nM JNK inhibitor SP600125. When used, SP600125 was added 1 h before and maintained throughout the incubation period. After incubation, Nox-4 mRNA expression levels were determined by real-time RT-PCR. The bars are means ± the SD of the relative expression of Nox-4 versus α-actin mRNA levels from three separate experiments. (D) SMCs were exposed to 0 or 40 μg of 7-Kchol/ml for 24 h with 0 (control) or 40 nM JNK inhibitor SP600125. Lysates were then immunoblotted for Nox-4, CHOP/GADD 153, and GRP78/Bip, and α-actin was used as internal standard.

hypercholesterolemic patients (19) and cholesterol-fed rabbits (41).

The constitutively active Nox proteins, which produce low levels of ROS under basal conditions, can be upregulated in the vascular wall by proinflammatory factors, such as growth factors and cytokines (16, 47). Numerous agonists of ROS production involved in atheromatous plaque progression, such as angiotensin II, PDGF, proinflammatory cytokines, and oxidized LDL (for a review, see reference 25), differentially modulate Nox expression. Chronic infusion of angiotensin II induces the expression of both Nox-1 and Nox-4 proteins in the rat aorta (36, 53), whereas Nox-1 and Nox-4 mRNAs are differently regulated in rat SMCs by angiotensin II, PDGF, and phorbol myristate acetate (26). Nox-4 mRNA has also been shown to be upregulated during the atheroma stage of the plaque containing an abundance of SMCs, whereas the expression of Nox-1 remains low in intact human coronary arteries and isolated vascular cells (45). The differences in the levels of Nox proteins detected in SMCs within atherosclerotic lesions may reflect distinct modes of regulation and/or differences in the subcellular localization. The intracellular location of the Nox-4 protein was previously based on predictions made using the PSORT program, which seemed to localize Nox-4 predominantly in the ER (20, 26). Recently, Hilenski et al. (18) reported that Nox-4 in fact localizes in the nucleus and colocalizes with vinculin in focal adhesion sites in rat vascular SMCs. Here we show that Nox-4 is found in both the ER membranes and the nuclei of SMCs. Control experiments with the synthetic peptide used to immunize rabbits and Western blotting have both confirmed the specificity of the anti-human Nox-4 antibody used in the present study. This means that we cannot exclude the possibility that the difference in the pattern of Nox

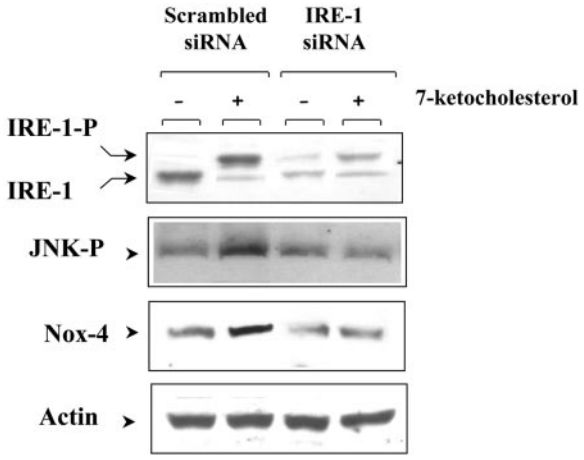

FIG. 9. IRE-1 controls the 7-Kchol-induced expression of Nox-4. SMCs were transfected with scrambled siRNA or IRE-1 siRNA duplexes. After incubation for 24 h in complete medium, SMCs were exposed to 0 or 40 μg of 7-Kchol/ml for 16 h. The IRE-1 protein was detected by Western blot analysis with the anti-IRE-1 antibody, which recognizes both the wild-type (IRE-1) and the phosphorylated forms (IRE-1-P) of IRE-1. Cells lysates were analyzed by Western blotting with antibodies directed against JNK phospho-specific Thr^{183} and Tyr^{185}, Nox-4, and α-actin. The Western blots shown are representative of three separate experiments.

immunolabeling is due to species specificity (rat versus human origin). Consistent with the subcellular localization of Nox-4 in SMCs, the results from real-time imaging analyzed by confocal microscopy revealed that 7-Kchol induces focal intracellular ROS production in paranuclear and nuclear regions that depends closely on Nox-4 expression, as demonstrated by Nox-4 silencing and experiments with the NAD(P)H inhibitor DPI.

The data from the present study provide strong evidence that Nox-4 is involved in the onset of 7-Kchol-induced apoptosis. Recent studies have suggested that the cell damage induced by 7-Kchol, which can be prevented by antioxidant agents such as glutathione, *N*-acetylcysteine and vitamin E may be due to ROS production (28, 29). Here we show that 7-Kchol-treated SMCs undergo apoptosis characterized by phosphatidylserine externalization, loss of mitochondrial transmembrane potential, modification of both antiapoptotic Bcl-2 and proapoptotic Bax expression, and caspase activation. These findings concur with previous studies that have identified downstream apoptotic effects of oxysterols in other cell types (9, 28, 39, 43). The loss of Nox-4 expression in SMCs transfected with the Nox-4 siRNA markedly reduces 7-Kchol-induced apoptotic events, suggesting that this oxidase plays a key role in regulating SMC death. Furthermore, 7-Kchol-dependent Nox-4 expression is tied to the induction of both ER chaperone GRP78/Bip and cell death effector CHOP/GADD153, two markers of the ER stress-dependent UPR signaling pathway. This effect is abolished when Nox-4 expression is repressed by transfection with a specific Nox-4 siRNA. This indicates that the upregulation of Nox-4 by 7-Kchol may induce a dramatic disruption of redox homeostasis of ER, leading to apoptosis. Overexpression of these UPR hallmarks and early ER Ca^{2+} efflux have been induced in rat models of brain ischemia and/or reperfusion (40) and in ischemic kidney epithelial cells (10). Ares et al. (2, 3) reported that ER Ca^{2+} pools contribute to the oscillations seen in SMCs treated with both 7-β- and 25-hydroxycholesterol and that this results in the depletion of ER Ca^{2+} stores within a few hours. Our findings demonstrate that 7-Kchol rapidly modified the intracellular concentration of Ca^{2+} and induced Ca^{2+} oscillations in SMCs. This effect is independent of Nox-4 expression, since the Ca^{2+} oscillations induced by 7-Kchol are not affected in siRNA Nox-4-transfected SMCs. Several studies have indicated that there is a link between changes in cytosolic Ca^{2+} level and apoptotic events, but the precise role of Ca^{2+} on the various signaling pathways remains to be determined. Recent data have shown that accumulation of free cholesterol within macrophage ER membranes disturbs ER functions by depleting ER Ca^{2+} stores and by inducing the UPR (13). Feng et al. (13) have reported that the accumulation of free cholesterol resulted in a full range of apoptotic events and the subsequent activation of chaperones and CHOP factors leading to caspase-dependent cell death. Since a very similar scenario occurs in SMCs exposed to 7-Kchol, we suggest that this oxysterol may disturb membrane cholesterol homeostasis, which plays a decisive role in ER stability, an effect that has already been reported for 25-hydroxycholesterol in human fibroblasts (24). An excess of 7-Kchol, in addition to its suppressive effect on the rate of cholesterol biosynthesis, esterification, and cholesterol efflux (48, 54), may also induce a rapid expansion of the ER cholesterol pool, which could have an impact on several different ER functions. Thus, 7-Kchol may act directly or indirectly on a stressor of ER, thus resulting in the induction of the UPR and subsequent cell apoptosis. Our findings show that 7-Kchol activates one of the transducers of the UPR, IRE-1, and the downstream signaling pathways, which partially regulate both the adaptive survival and apoptotic pathways. Multiple overlapping pathways, both proapoptotic and antiapoptotic, which are induced by ER stress and mediated by IRE-1, may be implicated in the cytotoxicity of 7-Kchol. Here we provide the first evidence that 7-Kchol promotes Nox-4 expression by stimulating the IRE-1/JNK/AP-1 signaling pathway. Silencing of IRE-1 by an siRNA strategy or inhibition of JNK activity suppressed Nox-4 expression and protected SMCs from 7-Kchol-induced cell death. This demonstrates that Nox-4 expression, which is essential for the ER-stress-induced cell death triggered by 7-Kchol, is controlled by the IRE-1 signaling pathway. Although we still do not know how Nox-4 acts on downstream targets to induce cell death, the Nox-4 silencing experiments clearly show that, of several UPR-inducible proapoptotic effectors identified, it is Nox-4 that modulates the expression of CHOP.

In conclusion, these findings highlight the role of nonphagocytic NAD(P)H oxidase proteins in the activation of multiple intracellular signaling pathways and in the onset of atherosclerosis (16). In addition, the present study also opens new avenues of research into the Nox proteins, especially into Nox-4, which could offer a potential therapeutic target for new drugs developed for use in cardiovascular diseases.

ACKNOWLEDGMENTS

We thank G. Peranzi for assistance with confocal microscopy and P. Rouet-Benzineb (INSERM U410) and D. Bernuau (INSERM U327)

for the NF-κB-luciferase and the AP-1-luciferase plasmids, respectively.

This study was supported by the Institut National de la Santé et de la Recherche Médicale (INSERM) and in part by grants from the Conseil Régional de Bourgogne and the Association pour la Recherche sur le Cancer (EOD 5831).

REFERENCES

1. **Andreassi, M. G., and N. Botto.** 2003. DNA damage as a new emerging risk factor in atherosclerosis. Trends Cardiovasc. Med. **13:**270–275.
2. **Ares, M. P., M. I. Porn-Ares, S. Moses, J. Thyberg, L. Juntti-Berggren, P. Berggren, A. Hultgardh-Nilsson, B. Kallin, and J. Nilsson.** 2000. 7β-Hydroxycholesterol induces Ca^{2+} oscillations, MAP kinase activation, and apoptosis in human aortic smooth muscle cells. Atherosclerosis **153:**23–35.
3. **Ares, M. P., M. I. Porn-Ares, J. Thyberg, L. Juntti-Berggren, P. O. Berggren, U. Diczfalusy, B. Kallin, I. Bjorkhem, S. Orrenius, and J. Nilsson.** 1997. Ca^{2+} channel blockers verapamil and nifedipine inhibit apoptosis induced by 25-hydroxycholesterol in human aortic smooth muscle cells. J. Lipid Res. **38:**2049–2061.
4. **Baeuerle, P. A., and D. Baltimore.** 1996. NF-κB: ten years after. Cell **87:**13–20.
5. **Banfi, B., A. Maturana, S. Jaconi, S. Arnaudeau, T. Laforge, B. Sinha, E. Ligeti, N. Demaurex, and K. H. Krause.** 2000. A mammalian H+ channel generated through alternative splicing of the NADPH oxidase homolog NOH-1. Science **287:**138–142.
6. **Bjorkhem, I., and U. Diczfalusy.** 2002. Oxysterols: friends, foes, or just fellow passengers? Arterioscler. Thromb. Vasc. Biol. **22:**734–742.
7. **Brenner, D. A., M. O'Hara, P. Angel, M. Chojkier, and M. Karin.** 1989. Prolonged activation of jun and collagenase genes by tumour necrosis factor alpha. Nature **337:**661–663.
8. **Brewer, J. W., J. L. Cleveland, and L. M. Hendershot.** 1997. A pathway distinct from the mammalian unfolded protein response regulates expression of endoplasmic reticulum chaperones in non-stressed cells. EMBO J. **16:**7207–7216.
9. **Brown, A. J., and W. Jessup.** 1999. Oxysterols and atherosclerosis. Atherosclerosis **142:**1–28.
10. **Bush, K. T., S. H. Keller, and S. K. Nigam.** 2000. Genesis and reversal of the ischemic phenotype in epithelial cells. J. Clin. Investig. **106:**621–626.
11. **Cheng, G., Z. Cao, X. Xu, E. G. van Meir, and J. D. Lambeth.** 2001. Homologs of gp91phox: cloning and tissue expression of Nox3, Nox4, and Nox5. Gene **269:**131–140.
12. **de Nigris, F., A. Lerman, L. J. Ignarro, S. Williams-Ignarro, V. Sica, A. H. Baker, L. O. Lerman, Y. J. Geng, and C. Napoli.** 2003. Oxidation-sensitive mechanisms, vascular apoptosis, and atherosclerosis. Trends Mol. Med. **9:**351–359.
13. **Feng, B., P. M. Yao, Y. Li, C. M. Devlin, D. Zhang, H. P. Harding, M. Sweeney, J. X. Rong, G. Kuriakose, E. A. Fisher, A. R. Marks, D. Ron, and I. Tabas.** 2003. The endoplasmic reticulum is the site of cholesterol-induced cytotoxicity in macrophages. Nat. Cell Biol. **5:**781–792.
14. **Geiszt, M., J. B. Kopp, P. Varnai, and T. L. Leto.** 2000. Identification of renox, an NAD(P)H oxidase in kidney. Proc. Natl. Acad. Sci. USA **97:**8010–8014.
15. **Green, D., and G. Kroemer.** 1998. The central executioners of apoptosis: caspases or mitochondria? Trends Cell Biol. **8:**267–271.
16. **Griendling, K. K., D. Sorescu, and M. Ushio-Fukai.** 2000. NAD(P)H oxidase: role in cardiovascular biology and disease. Circ. Res. **86:**494–501.
17. **Guzik, T. J., N. E. West, E. Black, D. McDonald, C. Ratnatunga, R. Pillai, and K. M. Channon.** 2000. Vascular superoxide production by NAD(P)H oxidase: association with endothelial dysfunction and clinical risk factors. Circ. Res. **86:**E85–E90.
18. **Hilenski, L. L., R. E. Clempus, M. T. Quinn, J. D. Lambeth, and K. K. Griendling.** 2004. Distinct subcellular localizations of Nox1 and Nox4 in vascular smooth muscle cells. Arterioscler. Thromb. Vasc. Biol. **24:**677–683.
19. **Hodis, H. N., D. W. Crawford, and A. Sevanian.** 1991. Cholesterol feeding increases plasma and aortic tissue cholesterol oxide levels in parallel: further evidence for the role of cholesterol oxidation in atherosclerosis. Atherosclerosis **89:**117–126.
20. **Kalinina, N., A. Agrotis, E. Tararak, Y. Antropova, P. Kanellakis, O. Ilyinskaya, M. T. Quinn, V. Smirnov, and A. Bobik.** 2002. Cytochrome b558-dependent NAD(P)H oxidase-phox units in smooth muscle and macrophages of atherosclerotic lesions. Arterioscler. Thromb. Vasc. Biol. **22:**2037–2043.
21. **Kaufman, R. J.** 1999. Stress signaling from the lumen of the endoplasmic reticulum: coordination of gene transcriptional and translational controls. Genes Dev. **13:**1211–1233.
22. **Kockx, M. M., and A. G. Herman.** 2000. Apoptosis in atherosclerosis: beneficial or detrimental? Cardiovasc. Res. **45:**736–746.
23. **Lambeth, J. D., G. Cheng, R. S. Arnold, and W. A. Edens.** 2000. Novel homologs of gp91phox. Trends Biochem. Sci. **25:**459–461.
24. **Lange, Y., J. Ye, M. Rigney, and T. L. Steck.** 1999. Regulation of endoplasmic reticulum cholesterol by plasma membrane cholesterol. J. Lipid Res. **40:**2264–2270.
25. **Lassegue, B., and R. E. Clempus.** 2003. Vascular NAD(P)H oxidases: specific features, expression, and regulation. Am. J. Physiol. Regul. Integr. Comp. Physiol. **285:**R277–R297.
26. **Lassegue, B., D. Sorescu, K. Szocs, Q. Yin, M. Akers, Y. Zhang, S. L. Grant, J. D. Lambeth, and K. K. Griendling.** 2001. Novel $gp91^{phox}$ homologues in vascular smooth muscle cells: nox1 mediates angiotensin II-induced superoxide formation and redox-sensitive signaling pathways. Circ. Res. **88:**888–894.
27. **Littlewood, T. D., and M. R. Bennett.** 2003. Apoptotic cell death in atherosclerosis. Curr. Opin. Lipidol. **14:**469–475.
28. **Lizard, G., S. Gueldry, O. Sordet, S. Monier, A. Athias, C. Miguet, G. Bessede, S. Lemaire, E. Solary, and P. Gambert.** 1998. Glutathione is implied in the control of 7-ketocholesterol-induced apoptosis, which is associated with radical oxygen species production. FASEB J. **12:**1651–1663.
29. **Lizard, G., C. Miguet, G. Bessede, S. Monier, S. Gueldry, D. Neel, and P. Gambert.** 2000. Impairment with various antioxidants of the loss of mitochondrial transmembrane potential and of the cytosolic release of cytochrome *c* occurring during 7-ketocholesterol-induced apoptosis. Free Radic. Biol. Med. **28:**743–753.
30. **Lizard, G., S. Monier, C. Cordelet, L. Gesquiere, V. Deckert, S. Gueldry, L. Lagrost, and P. Gambert.** 1999. Characterization and comparison of the mode of cell death, apoptosis versus necrosis, induced by 7β-hydroxycholesterol and 7-ketocholesterol in the cells of the vascular wall. Arterioscler. Thromb. Vasc. Biol. **19:**1190–1200.
31. **Mallat, Z., and A. Tedgui.** 2000. Apoptosis in the vasculature: mechanisms and functional importance. Br. J. Pharmacol. **130:**947–962.
32. **Martinet, W., D. M. Schrijvers, G. R. De Meyer, J. Thielemans, M. W. Knaapen, A. G. Herman, and M. M. Kockx.** 2002. Gene expression profiling of apoptosis-related genes in human atherosclerosis: upregulation of death-associated protein kinase. Arterioscler. Thromb. Vasc. Biol. **22:**2023–2029.
33. **McCullough, K. D., J. L. Martindale, L. O. Klotz, T. Y. Aw, and N. J. Holbrook.** 2001. Gadd153 sensitizes cells to endoplasmic reticulum stress by down-regulating Bcl2 and perturbing the cellular redox state. Mol. Cell. Biol. **21:**1249–1259.
34. **Miguet, C., S. Monier, A. Bettaieb, A. Athias, G. Bessede, A. Laubriet, S. Lemaire, D. Neel, P. Gambert, and G. Lizard.** 2001. Ceramide generation occurring during 7β-hydroxycholesterol- and 7-ketocholesterol-induced apoptosis is caspase independent and is not required to trigger cell death. Cell Death Differ. **8:**83–99.
35. **Miguet-Alfonsi, C., C. Prunet, S. Monier, G. Bessede, S. Lemaire-Ewing, A. Berthier, F. Menetrier, D. Neel, P. Gambert, and G. Lizard.** 2002. Analysis of oxidative processes and of myelin figures formation before and after the loss of mitochondrial transmembrane potential during 7β-hydroxycholesterol and 7-ketocholesterol-induced apoptosis: comparison with various pro-apoptotic chemicals. Biochem. Pharmacol. **64:**527–541.
36. **Mollnau, H., M. Wendt, K. Szocs, B. Lassegue, E. Schulz, M. Oelze, H. Li, M. Bodenschatz, M. August, A. L. Kleschyov, N. Tsilimingas, U. Walter, U. Forstermann, T. Meinertz, K. Griendling, and T. Munzel.** 2002. Effects of angiotensin II infusion on the expression and function of NAD(P)H oxidase and components of nitric oxide/cGMP signaling. Circ. Res. **90:**E58–E65.
37. **Monier, S., M. Samadi, C. Prunet, M. Denance, A. Laubriet, A. Athias, A. Berthier, E. Steinmetz, G. Jurgens, A. Negre-Salvayre, G. Bessede, S. Lemaire-Ewing, D. Neel, P. Gambert, and G. Lizard.** 2003. Impairment of the cytotoxic and oxidative activities of 7β-hydroxycholesterol and 7-ketocholesterol by esterification with oleate. Biochem. Biophys. Res. Commun. **303:**814–824.
38. **Pahl, H. L., and P. A. Baeuerle.** 1997. The ER-overload response: activation of NF-κB. Trends Biochem. Sci. **22:**63–67.
39. **Panini, S. R., and M. S. Sinensky.** 2001. Mechanisms of oxysterol-induced apoptosis. Curr. Opin. Lipidol. **12:**529–533.
40. **Paschen, W.** 2001. Dependence of vital cell function on endoplasmic reticulum calcium levels: implications for the mechanisms underlying neuronal cell injury in different pathological states. Cell Calcium **29:**1–11.
41. **Rong, J. X., L. Shen, Y. H. Chang, A. Richters, H. N. Hodis, and A. Sevanian.** 1999. Cholesterol oxidation products induce vascular foam cell lesion formation in hypercholesterolemic New Zealand White rabbits. Arterioscler. Thromb. Vasc. Biol. **19:**2179–2188.
42. **Rusinol, A. E., L. Yang, D. Thewke, S. R. Panini, M. F. Kramer, and M. S. Sinensky.** 2000. Isolation of a somatic cell mutant resistant to the induction of apoptosis by oxidized low-density lipoprotein. J. Biol. Chem. **275:**7296–7303.
43. **Rusinol, A. R., D. Thewke, J. Liu, N. Freeman, S. R. Panini, and M. S. Sinensky.** 2004. Akt/PKB regulation of Bcl family members during oxysterol induced apoptosis. J. Biol. Chem. **279:**1392–1399.
44. **Shi, Y., R. Niculescu, D. Wang, S. Patel, K. L. Davenpeck, and A. Zalewski.** 2001. Increased NAD(P)H oxidase and reactive oxygen species in coronary arteries after balloon injury. Arterioscler. Thromb. Vasc. Biol. **21:**739–745.
45. **Sorescu, D., D. Weiss, B. Lassegue, R. E. Clempus, K. Szocs, G. P. Sorescu, L. Valppu, M. T. Quinn, J. D. Lambeth, J. D. Vega, W. R. Taylor, and K. K. Griendling.** 2002. Superoxide production and expression of nox family proteins in human atherosclerosis. Circulation **105:**1429–1435.
46. **Suh, Y. A., R. S. Arnold, B. Lassegue, J. Shi, X. Xu, D. Sorescu, A. B. Chung,**

K. K. Griendling, and J. D. Lambeth. 1999. Cell transformation by the superoxide-generating oxidase Mox1. Nature **401:**79–82.
47. **Szocs, K., B. Lassegue, D. Sorescu, L. L. Hilenski, L. Valppu, T. L. Couse, J. N. Wilcox, M. T. Quinn, J. D. Lambeth, and K. K. Griendling.** 2002. Upregulation of Nox-based NAD(P)H oxidases in restenosis after carotid injury. Arterioscler. Thromb. Vasc. Biol. **22:**21–27.
48. **Tabas, I.** 2002. Consequences of cellular cholesterol accumulation: basic concepts and physiological implications. J. Clin. Investig. **110:**905–911.
49. **Tobiume, K., A. Matsuzawa, T. Takahashi, H. Nishitoh, K. Morita, K. Takeda, O. Minowa, K. Miyazono, T. Noda, and H. Ichijo.** 2001. ASK1 is required for sustained activations of JNK/p38 MAP kinases and apoptosis. EMBO Rep. **2:**222–228.
50. **Treiman, M.** 2002. Regulation of the endoplasmic reticulum calcium storage during the unfolded protein response–significance in tissue ischemia? Trends Cardiovasc. Med. **12:**57–62.
51. **Urano, F., X. Wang, A. Bertolotti, Y. Zhang, P. Chung, H. P. Harding, and D. Ron.** 2000. Coupling of stress in the ER to activation of JNK protein kinases by transmembrane protein kinase IRE1. Science **287:**664–666.
52. **Wei, M. C., W. X. Zong, E. H. Cheng, T. Lindsten, V. Panoutsakopoulou, A. J. Ross, K. A. Roth, G. R. MacGregor, C. B. Thompson, and S. J. Korsmeyer.** 2001. Proapoptotic BAX and BAK: a requisite gateway to mitochondrial dysfunction and death. Science **292:**727–730.
53. **Wingler, K., S. Wunsch, R. Kreutz, L. Rothermund, M. Paul, and H. H. Schmidt.** 2001. Upregulation of the vascular NAD(P)H-oxidase isoforms Nox1 and Nox4 by the renin-angiotensin system in vitro and in vivo. Free Radic. Biol. Med. **31:**1456–1464.
54. **Zhang, Y., C. Yu, J. Liu, T. A. Spencer, C. C. Chang, and T. Y. Chang.** 2003. Cholesterol is superior to 7-ketocholesterol or 7α-hydroxycholesterol as an allosteric activator for acyl-coenzyme A:cholesterol acyltransferase 1. J. Biol. Chem. **278:**11642–11647.
55. **Zhou, Q., E. Wasowicz, B. Handler, L. Fleischer, and F. A. Kummerow.** 2000. An excess concentration of oxysterols in the plasma is cytotoxic to cultured endothelial cells. Atherosclerosis **149:**191–197.
56. **Zinszner, H., M. Kuroda, X. Wang, N. Batchvarova, R. T. Lightfoot, H. Remotti, J. L. Stevens, and D. Ron.** 1998. CHOP is implicated in programmed cell death in response to impaired function of the endoplasmic reticulum. Genes Dev. **12:**982–995.